Neuron
Article

# A Tale of Two Retinal Domains: Near-Optimal Sampling of Achromatic Contrasts in Natural Scenes through Asymmetric Photoreceptor Distribution

Tom Baden,[1,2,5] Timm Schubert,[1,5] Le Chang,[1,3] Tao Wei,[1] Mariana Zaichuk,[1] Bernd Wissinger,[4] and Thomas Euler[1,2,*]
[1]Werner Reichardt Centre for Integrative Neurosciences (CIN)/Institute for Ophthalmic Research, University of Tübingen, Otfried-Müller-Strasse 25, 72076 Tübingen, Germany
[2]Bernstein Centre for Computational Neuroscience (BCCN), University of Tübingen, Otfried-Müller-Strasse 25, 72076 Tübingen, Germany
[3]Institute of Biophysics, Chinese Academy of Sciences, 15 Datun Road, Chaoyang District, Beijing 100101, China
[4]Molecular Genetics Laboratory, Centre for Ophthalmology, University of Tübingen, Röntgenweg 11, 72076 Tübingen, Germany
[5]These authors contributed equally to this work
*Correspondence: thomas.euler@cin.uni-tuebingen.de
http://dx.doi.org/10.1016/j.neuron.2013.09.030

## SUMMARY

**For efficient coding, sensory systems need to adapt to the distribution of signals to which they are exposed. In vision, natural scenes above and below the horizon differ in the distribution of chromatic and achromatic features. Consequently, many species differentially sample light in the sky and on the ground using an asymmetric retinal arrangement of short- (S, "blue") and medium- (M, "green") wavelength-sensitive photoreceptor types. Here, we show that in mice this photoreceptor arrangement provides for near-optimal sampling of natural achromatic contrasts. Two-photon population imaging of light-driven calcium signals in the synaptic terminals of cone-photoreceptors expressing a calcium biosensor revealed that S, but not M cones, preferred dark over bright stimuli, in agreement with the predominance of dark contrasts in the sky but not on the ground. Therefore, the different cone types do not only form the basis of "color vision," but in addition represent distinct (achromatic) contrast-selective channels.**

## INTRODUCTION

In terrestrial visual scenes, the horizon divides two distinct domains differing in both spectral composition and the distribution of achromatic contrasts (Gouras and Ekesten, 2004; Laughlin and McGinness, 1978; Ratliff et al., 2010). Moreover, visual stimuli of particular behavioral importance often occur exclusively in one visual domain, such as an aerial predator approaching from above (Gouras and Ekesten, 2004; Nikonov et al., 2006). Presumably as an evolutionary consequence, a broad range of different vertebrates and invertebrates, including diverse species, such as guinea pigs, rabbits, hyenas, guppies, dragonflies, or honey bee drones, possess unequal distributions of photoreceptor types in different retinal domains (Calderone and Jacobs, 1995; Jacobs, 1993; Laughlin and McGinness, 1978; Peichl, 2005; Röhlich et al., 1994; Szél et al., 1994; Weckström and Laughlin, 1995; Yin et al., 2006).

The mouse cone photoreceptor array features a pronounced dorsoventral gradient in opsin expression (Szél et al., 1992): medium wavelength-sensitive (M) cones coexpress short wavelength-sensitive (S) opsin, the extent of which increases toward the ventral edge of the retina (Röhlich et al., 1994). Measurements at the level of the opsin mRNA and electroretinograms (ERGs) indicated that across the entire retina S opsin outnumbers M opsin (Applebury et al., 2000; Jacobs and Williams, 2007; Jacobs et al., 2004; Lyubarsky et al., 1999). As all "evolutionary" M cones in mice likely coexpress S opsin, for simplicity we refer to them in the following as coexpressing cones or "MS cones." Exclusively S opsin-expressing cones ("true" S cones) are homogenously distributed across the retina (Haverkamp et al., 2005) and make up only ~4% of all cones. Recordings from bipolar cells (Breuninger et al., 2011) and retinal ganglion cells (Chang et al., 2013; Ekesten and Gouras, 2005; Wang et al., 2011) demonstrated that the opsin coexpression gradient results in a dramatic functional dorsoventral division of the mouse retina with respect to spectral tuning, consistent with data from multifocal ERGs (Calderone and Jacobs, 1995). As a consequence, the mouse retina can be divided into three major functional regions: (1) the dorsal retina, containing mainly MS cones with very little S opsin coexpression, interspersed with "true" S cones, (2) a relatively narrow central "opsin transitional zone" (Chang et al., 2013; Wang et al., 2011), in which the S/M opsin coexpression ratio increases, and (3) the strongly S opsin-dominated ventral retina.

Although behavioral experiments demonstrate that mice are able to discriminate colors (Jacobs et al., 2004), little is known about the functional consequences of the dorsoventral retinal subdivision with respect to the visual environment. It has been proposed that the match in opsin spectral sensitivity and predominant "color" distribution may be beneficial for visual coding, in particular, with respect to ecological niches and natural behaviors (reviewed in Peichl, 2005). Indeed, it is tempting to draw a simple connection between "green" and "blue" vision

and terrestrial natural scenes: the dorsal retina, which samples light in the lower visual field, is mainly "green" sensitive, whereas the ventral retina, which samples light in the upper visual field, is mainly "blue" sensitive—in line with a "blue sky" and "greenish ground" (Gouras and Ekesten, 2004; Szél et al., 1994, 2000). However, the extent to which the opsin expression gradient benefits the sampling of achromatic contrast statistics (Yin et al., 2009) in the sky and on the ground has been little explored experimentally.

By combining two-photon imaging of light-evoked $Ca^{2+}$ changes in cone pedicles and immunohistochemistry, we show that, in mice, S opsin coexpression in MS cones in the ventral retina correlates with a fundamental change in response properties of these cones in the achromatic domain: unlike the dorsal, dominantly M opsin-expressing cones, which respond to light and dark flashes with equal and opposite gain, strongly S opsin-coexpressing MS cones in the ventral retina preferentially encode dark contrasts. Using computational modeling and information theory, we show that this preference for dark contrasts is optimal to sample the achromatic contrast distribution in natural scenes above the horizon. Our data suggest that it is not the earlier proposed match in "color" between retinal opsin expression and visual domains in the environment that improves visual encoding, but the difference in (achromatic) cone response properties.

## RESULTS

### A Predominance of Dark Contrasts in the Sky

Visual scenes in the sky and on the ground differ in achromatic contrast statistics (e.g., Karklin and Lewicki, 2009; Ratliff et al., 2010). Against the bright backdrop of the daylight sky, most objects appear as negative (dark) contrasts, whereas on the ground positive (light) and dark contrasts are more balanced. To explore achromatic contrast statistics in "mouse-view" natural scenes that acknowledge the spectral properties of mouse M and S opsins (Jacobs et al., 1991), we built a simple "hyperspectral scanner" based on a UV-capable spectrometer (Figure S1A available online). "Pixels" were sequentially sampled in space by two RC-servo motors rotating the spectrometer head in yaw and tilt to generate images of natural scenes containing information of the luminance distribution across the spectrum from 350 to 1,040 nm. To approximate the spatial resolution of the mouse eye (Prusky and Douglas, 2008), "hyperspectral images" were sampled at a resolution of 1° visual angle, corresponding to approximately ten cones on the mouse retina. Note that for our purpose, that is, calculating contrast distribution of natural scenes (see next paragraph), matching the spatial sampling density exactly to that of mice is not necessary because moderate changes in sampling point density bears little effect on contrast calculation. This can be intuitively understood by taking a photograph of a natural scene followed by spatial downsampling—the histogram of the brightness distribution remains almost unchanged. For each "pixel," the relative activation of S and M opsins was then estimated based on their absorption spectra (Figure S1B). This allowed reconstructing a spectrographic "mouse-view" image of an early spring daytime forest scene based on the absorption of mouse cone opsins (Figure 1A), or

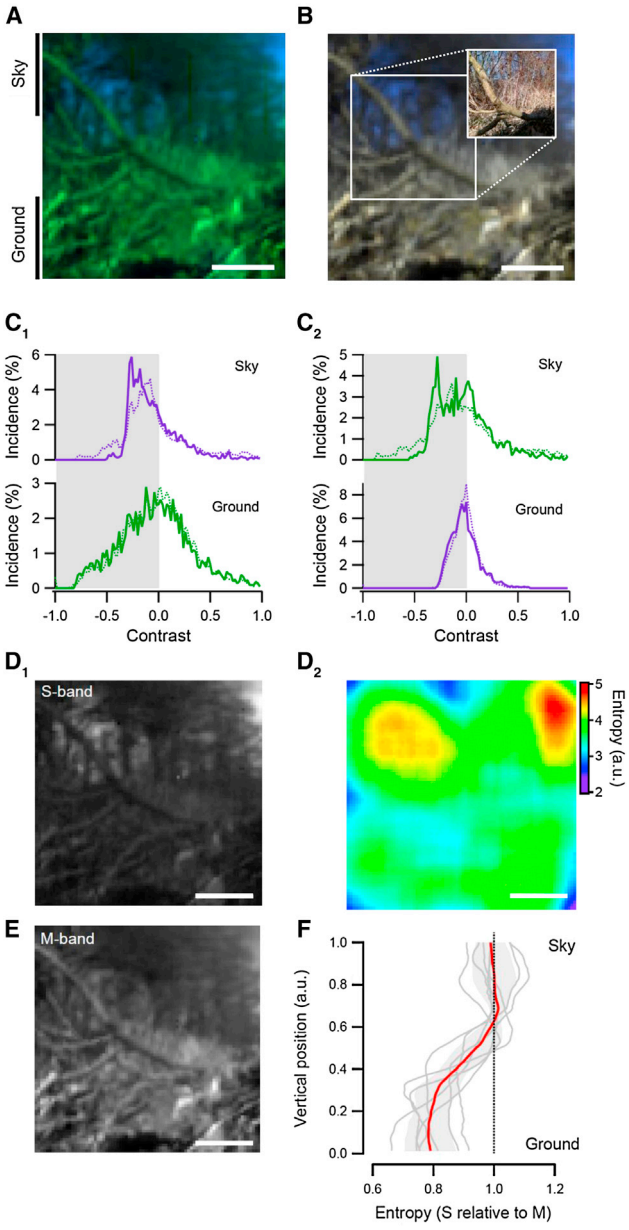


**Figure 1. "Mouse-View" Natural Scenes**

(A and B) (A) "Mouse-view" and (B) "human-view" image of an early spring daytime forest scene reconstructed using data from the "hyperspectral scanner" (see Figure S1 for details). Inset: photograph illustrating the recorded scene; scale bar: 20° visual angle.

(C) ($C_1$) shows contrast distribution in "mouse-view" images in the "S opsin band" in the sky (top) and in the "M opsin band" on the ground (bottom) for image in A (solid lines) and average from five images (dashed lines). ($C_2$) shows respective contrast distribution as sampled by $_F$M cones in the sky and $_F$S cones on the ground.

(D and E) Image contrast present in different spectral bands defined by S ($D_1$) and M opsin (E) spectra (Figure S1B) and ($D_2$), local image entropy calculated from ($D_1$). A higher local entropy indicates a higher local contrast.

(F) Mean S-band entropy is lower than S-band entropy on the ground but approximately equal to M entropy in the sky (red trace, mean S/M entropy ratio; gray shading, ±1 SEM; n = 7 "mouse-view" images).

See also Figure S1.

reconstructing the same scene matched to trichromatic human color vision (Figures 1B and S1C).

Across seven "mouse-view" images, estimated M opsin activation was ~10–13 times stronger than S opsin activation both in the sky and on the ground. This was partially due to a global predominance of medium-to-long wavelength light across the entire visual field (Wyszecki and Stiles, 2000). However, S opsin activation was relatively stronger in the sky than on the ground, whereas M opsin activation was approximately balanced for the two visual domains (data not shown). From the "mouse-view" images, we calculated the probability distribution of natural contrast levels (see Experimental Procedures) based on S opsin activation ("S-band") in the upper and M opsin activation ("M-band") in the lower visual fields. These data confirmed that in both the S- and the M-band, dark contrasts are much more prominent in the sky (i.e., the contrast distribution is biased to negative values), whereas the distribution of dark and light contrasts is roughly balanced on the ground (Figures 1$C_1$ and 1$C_2$). We also calculated the probability distribution of contrast levels using natural scene images calibrated for "human-view" from a public image database (Tkačik et al., 2011) and found, consistent with our own measurements, a predominance of dark contrasts in the sky but more balanced contrasts on the ground (Figures S1D and S1E). Repeating the analysis with an image series from this database of the same scene taken from dusk till dawn, we confirmed that this difference in contrast distribution is largely independent of daytime (data not shown). Note that our data for contrasts on the ground are not in contradiction to an earlier study (Ratliff et al., 2010) that showed natural scenes in both sky and ground to be dominated by dark contrasts: Contrast distributions even on the ground in mouse-view images exhibited a small but significant ($p = 0.02$) skew to negative values.

Taking into account the dorsoventral opsin gradient, for "optimized" sampling of the observed contrast distribution the mouse retina is expected to predominately sample dark contrasts in the sky using S opsin-expressing cones, and the approximately balanced contrast distribution on the ground using the predominantly M opsin-expressing cones (Figure 1$C_1$). In addition, contrast distribution on the ground was narrower in the S band (Figure 1$C_2$, bottom) than in the M band (Figure 1$C_1$, bottom), suggesting that the sampling of short wavelength light reflected from the ground provides for comparatively poor contrast discrimination (when assuming comparable signal-to-noise [S/N] levels in individual cones). To test this hypothesis, we spectrally filtered the mouse-view images using the S-band (Figure 1$D_1$) or the M band (Figure 1E) and estimated information "richness" (with respect to local contrast) from the entropy distribution in the images. Indeed, S-band images (Figure 1$D_1$) exhibited higher entropy in the sky than on the ground (Figure 1$D_2$). In comparison, M-band images (Figure 1E) were more balanced along the dorsoventral axis. Across seven "mouse-view" images, S-band entropy was consistently lower than M-band entropy on the ground, but approximately equal to M-band entropy in the sky (Figure 1F). Overall, this suggests that the opsin expression gradient along the dorsal-ventral axis of the mouse retina (Szél et al., 1992) is matched to an "information asymmetry" in natural scenes about the horizon, as suggested earlier (e.g., Szél et al., 1994). Notably, this vertical asymmetry appears to arise primarily from a lower-than-M entropy in the S-band on the ground, rather than a higher-than-M entropy in the sky (Figure 1F). In other words, if spectral selectivity were to be the only difference between M and S opsin-dominated cones, one may wonder why the mouse has evolved the strong S-band selectivity in the ventral retina, when M opsin-dominated cones would perform equally well. Taken together, our findings led us to ask how the specific cone arrangement combined with the contrast sampling properties of mouse cone types lends itself to differentially sample natural achromatic contrasts above and below the horizon.

## Anatomical Distribution of Cone Types in the Mouse Retina

To ensure that our transgenic biosensor mouse line (see next section) displays the known dorsoventral opsin coexpression gradient (Szél et al., 1992), we began by reassessing the opsin gradient at the anatomical level. To quantify the anatomical distribution of opsin expression in cones in the whole-mount retina, we used immunolabeling with antibodies against S and M opsins (Figure 2$A_1$). From such stainings, we estimated the opsin expression ratio of n = 38,916 individual cones, calculated as "M-S index" (MSi, see Experimental Procedures; Figure S2), with positive and negative MSi values denoting M and S opsin-labeling dominance, respectively. The MSi histogram revealed two distinctive peaks around 0.75 (55%) and −0.75 (17%), owing to the presence of cones predominately labeled for M or S opsin, respectively (Figure 2$A_2$). A third fraction of cones (28%) with a shallow MSi peak at approximately zero was attributed to cones with more balanced M and S opsin coexpression. The attribution of three distinct histochemical cone subtypes is supported by a significantly better fit of the data by a combination of three over two asymmetrical Gaussians (Figure 2B, see Experimental Procedures). The MSi distribution across the retina confirmed the striking dorsoventral separation of predominantly M- and S-expressing cones (Röhlich et al., 1994; Szél et al., 1992) (Figure 2C). Anatomically identified M cones ($_A$M) constituted >90% of all dorsal cones, but only ~20% in ventral retina (Figure 2D). In contrast, anatomically identified S cones ($_A$S) constituted <5% in dorsal retina and gradually increased toward ~50% of cones at the retina's ventral edge. The remaining cones were anatomically defined MS cones ($_A$MS), constituting ~5% of cones in dorsal retina, ~50% in central retina, and decreasing again toward the ventral edge. Note that the division into $_A$S, $_A$M, and $_A$MS cones was primarily used to compare estimated opsin expression ratios (i.e., MSi) to spectral contrast (SC) from functional measurements along the dorsoventral axis (see next section). Because of the low prevalence of "true" S cones in the mouse retina (Haverkamp et al., 2005), the large majority (>95%) of all three groups of cones ($_A$M, $_A$MS, $_A$S) are M/S-coexpressing cones varying in M/S opsin expression ratio.

## Functional Characterization of the Mouse Cone-Photoreceptor Array

As already suggested by earlier reports (Calderone and Jacobs, 1995; Chang et al., 2013; Wang et al., 2011), the functional

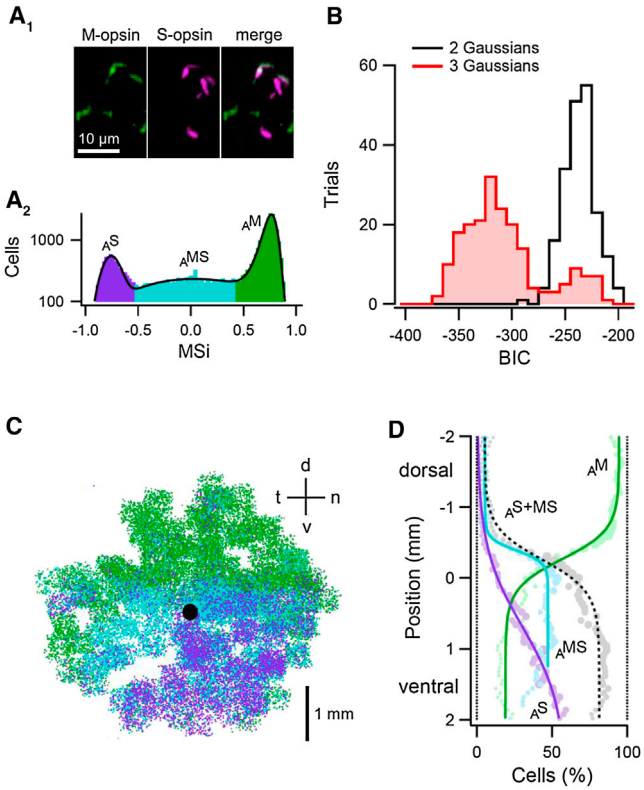


**Figure 2. Anatomical Cone-Type Distribution in the Mouse Retina**

($A_1$) Cone photoreceptor outer segments in the whole-mount retina immunolabeled for medium (M, "green") and short (S, "blue") wavelength-sensitive opsins.

($A_2$) Cone outer segments (n = 38,916 from three retinas) classified anatomically into $_A$M, $_A$S, and $_A$MS cones based on MSi (green, purple, cyan, respectively).

(B) The MSi distribution ($A_2$) is described better by three Gaussians than by two ($p < 0.001$). Lower values of Bayesian Information Criterion (BIC) denote a better fit (see Experimental Procedures).

(C) Spatial distribution of the three anatomical cone types across the retina (d, dorsal; v, ventral; t, temporal; n, nasal).

(D) Spatial profile along the dorsoventral axis, fitted with sigmoids. Marker size denotes the number of cells per bin.

See also Figure S2.

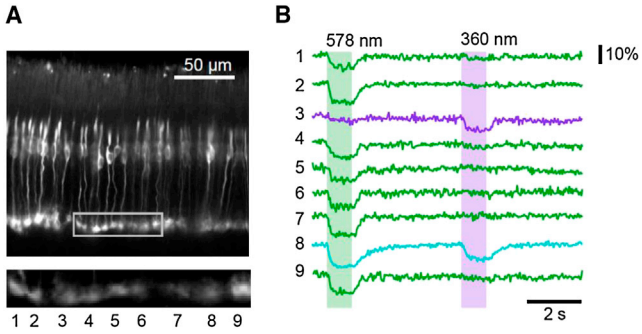


**Figure 3. Two-Photon Imaging of Light-Evoked $Ca^{2+}$ Signals in Cone Synaptic Terminals**

(A) Vertical slice with fluorescent cones expressing the ratiometric biosensor TN-XL in dorsal mouse retina of the HR2.1:TN-XL transgenic line (collapsed image stack; top) and enlarged image of cone pedicles (single optical section, bottom).

(B) Light-evoked $Ca^{2+}$ signals ($\Delta R/R$, averages of n = 8 trials) in the cone terminals shown in (A) to "green" and "blue" light flashes (shaded bars).

See also Figure S3.

consequences of the opsin gradient across the retina and of coexpression within single cones are difficult to judge from immunolabeling alone. Therefore, to assess how the opsin distribution is reflected in cone output we determined the distribution of functional cone types based on the spectral preference of their light responses. Using two-photon imaging (Denk and Detwiler, 1999; Denk et al., 1990), we recorded light-evoked $Ca^{2+}$ signals from individual cone synaptic terminals in retinal slices of HR2.1:TN-XL transgenic mice (Wei et al., 2012) (Figure 3). These mice express the ratiometric $Ca^{2+}$ biosensor TN-XL (Mank et al., 2006) exclusively in cones (Figure 3A) and provide for a high-throughput functional characterization of the cone array at single-synapse resolution (Figures 3B and 4). Notably, the monitoring of $Ca^{2+}$ directly within individual cone terminals brings about a number of advantages over electrical recordings (e.g., Nikonov et al., 2006). First, changes in presynaptic $Ca^{2+}$ are secondary to changes in electrical potential and are more directly related to the synaptic output with respect to glutamate release. Second, electrical recordings from cones are usually performed at the level of the cell body and thereby only indirectly reflect electrical activity within the cone pedicle. Third, during whole-cell recordings from cones the composition of the intracellular solution may change due to dialysis from the electrode and therefore could interfere with the generation of $Ca^{2+}$ signals. On the other hand, two-photon recordings within the retina may be confounded by direct and indirect activation of photosensitive cells by the laser and laser-evoked fluorescence (Denk and Detwiler, 1999; Euler et al., 2009; Wei et al., 2012). We therefore carefully examined the effect of laser-related activation of photopigments and found that in our recording situation (slices) and with sufficient background illumination from the light stimulator, the additional cone excitation due to laser-evoked effects is relatively weak and, more importantly, largely independent of cone type (see Discussion; Figure S3). Our approach therefore allowed us to study chromatic and contrast coding properties at the level of the individual cone's output, with presynaptic $Ca^{2+}$ as a proxy.

We recorded $Ca^{2+}$ signals evoked by "blue" (S, 360 nm, which is actually UVB) and "green" (M, 585 nm) sinusoidally modulated light in n = 1,996 cone terminals (Figure 4$A_1$) and calculated "spectral contrast" (SC; see Experimental Procedures) (Figure 4$A_2$, cf. Figure 2$A_2$). Functional cone types exhibited an overall spatial correspondence with anatomical cone types with dorsal M and ventral S dominance (Figures 4C and 4D, cf. 2C and 2D). However, unlike opsin expression ratios calculated from immunolabeling (Figure 2$A_2$), the SC distribution did not support the presence of a distinct functional cone phenotype with similar contributions from M and S opsins (Figure 4B). Instead, the functional response properties of individual cones fell into two populations: functional S cones ($_F$S, 67%) and functional M cones ($_F$M, 33%). Indeed, adding the spatial profiles of

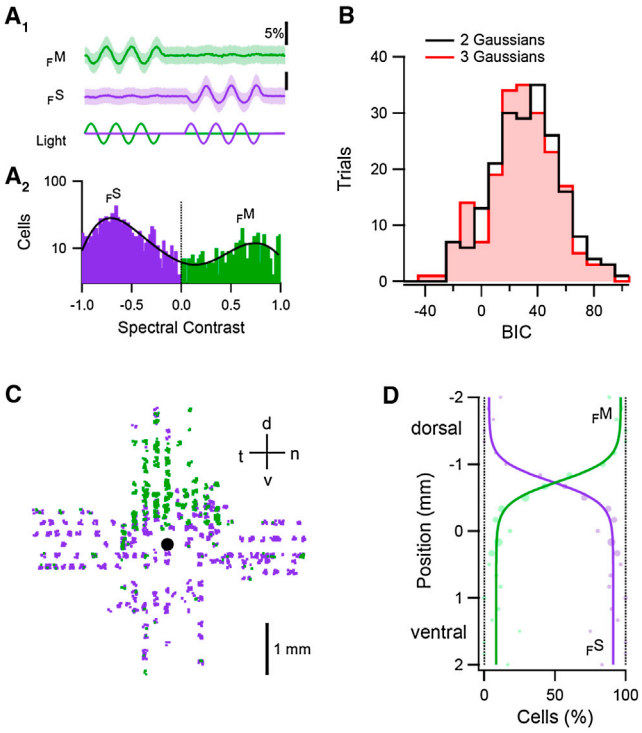


**Figure 4. Functional Cone-Type Distribution in the Mouse Retina**

($A_1$) Averaged $Ca^{2+}$ responses to a sinusoidal chromatic stimulus of $_F$M and $_F$S cones (n = 1,996 from 33 retinas, shadings ± 1 SEM), defined based on spectral contrast (SC, $A_2$).

(B) The SC histogram ($A_2$) is described equally well by the sum of two and three Gaussians (p > 0.5; see Experimental Procedures).

(C and D) Spatial distribution of two functional cone types across the retina (C) and spatial profile along the dorsoventral axis (D). Marker size denotes the number of cells per bin.

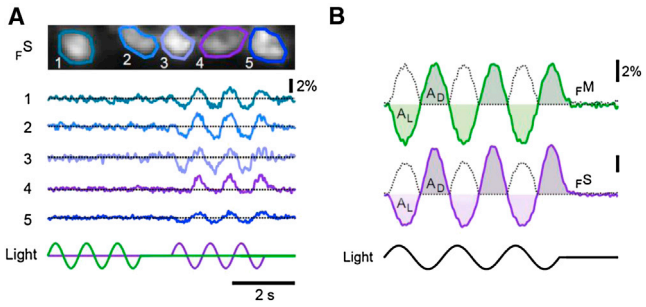


**Figure 5. Contrast Coding in $_F$M and $_F$S Cones Probed by Sinusoidal Stimuli**

(A) Average $Ca^{2+}$ responses (n = 6 trials) of individual neighboring $_F$S cone pedicles (top) to the chromatic stimulus used in Figure 4A.

(B) Average response of 118 $_F$M and 336 $_F$S cones. Shadings highlight response areas to light ($A_L$) and dark ($A_D$) episodes of the stimulus, and dashed lines indicate response modulus relative to baseline.

(anatomical) $_A$S and $_A$MS cones (Figure 2D, black dashed line) yields a similar distribution compared to (functional) $_F$S cones (Figure 4D). The transition from the $_F$M cone-dominated (≥67% $_F$M) dorsal retina to the $_F$S cone-dominated (≥67% $_F$S) ventral retina occurred within only ~400 μm (~14° of visual angle [Schaeffel, 2008]), which is in the range of estimates of the dorsoventral gradient profile based on our immunolabeling (Figure 2D), earlier immunodata (Röhlich et al., 1994), or retinal ganglion cell (RGC) data (Wang et al., 2011; for Discussion, see also Chang et al., 2013).

This result supports the predominance of S opsin in the mouse retina, in line with earlier findings yielded with other experimental approaches (Applebury et al., 2000; Calderone and Jacobs, 1995; Jacobs et al., 2004; Lyubarsky et al., 1999; Wang et al., 2011). Moreover, it appears that a large proportion of cones coexpressing M and S opsin simply exhibit a functional "S cone" phenotype, highlighting that cone function cannot be solely determined from opsin immunostainings (Calderone and Jacobs, 1995). This suggests that mice sample visual scenes below the horizon using mainly $_F$M cones, but, above the horizon using mainly $_F$S cones, the great majority of which are M/S-coexpressing cones.

## Contrast Coding by Functional S and M Cones

Do the contrast coding properties of $_F$S cones in the ventral retina (Figures 5 and 6) acknowledge the predominance of dark contrasts in the sky (Figure 1)? To address this question, we compared the responses to the light and dark episodes of the sinusoidally modulated stimulus used to determine chromatic preference (Figure 4). This revealed that many $_F$S cones did not encode dark and light with equal gain but instead preferentially encoded dark stimulus episodes (e.g., cone 4 in Figure 5A). On average, $_F$S cones exhibited a strong preference for dark stimulus episodes ($A_L$-$A_D$: −1.14 ± 2.05, $p < 0.001$, n = 336), whereas $_F$M cones responded to light and dark episode with equal and opposite amplitudes ($A_L$-$A_D$: −0.13 ± 1.21, $p > 0.05$, n = 118) (Figure 5B).

To more precisely estimate contrast coding by individual cones, we presented a pseudorandom sequence of chromatic dark and light flashes at different intensities from an intermediate light level (Figure 6A, left). The averaged responses of a cone to each contrast level were sorted by stimulus amplitude and then fitted to determine its individual stimulus-response curves ("gain functions," Figure 6A, right). In the examples shown, cones 1 (a $_F$M cone) and 2 (a $_F$S cone) responded to light and dark flashes with almost equal and opposite amplitude, whereas $_F$S cone 3 preferentially encoded dark flashes. To quantify contrast encoding for $_F$M and $_F$S cones at the population level, we calculated a "dark-light index," $DLi = (A_L - A_D)/(A_L + A_D)$, with $A_L$ and $A_D$ corresponding to the integrals of the gain curve below and above zero crossing, respectively (see Experimental Procedures). Accordingly, a DLi of 1 and −1 denotes cones exclusively responding to light or dark stimulus episodes, respectively, whereas a DLi of zero denotes a balanced response.

Gain functions estimated in a sample of 81 $_F$M cones and 148 $_F$S cones, sorted by DLi (Figure 6B), and average gain functions of all $_F$M and $_F$S cones (Figure 6C) revealed three striking differences in the way that $_F$M and $_F$S cones encoded contrast:

First, as a population, $_F$S cones were biased toward negative DLi values, whereas $_F$M cone DLi values were centered around

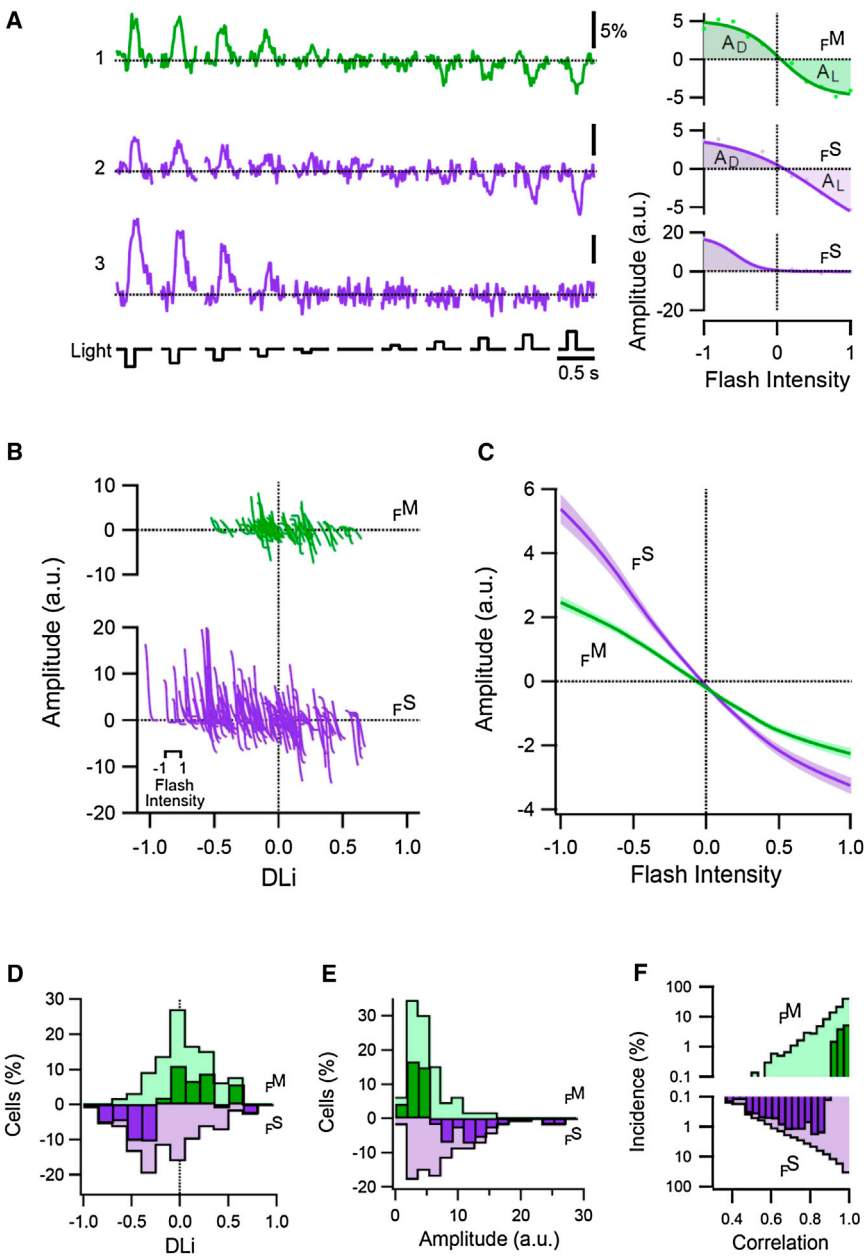


**Figure 6. Contrast Coding in $_F$M and $_F$S Cones Probed by Flash Stimuli**

(A) Average $Ca^{2+}$ responses (14 trials) of individual cones to different intensity light steps (left) and area under the responses ("amplitudes") as function of flash intensity fitted with sigmoids ("gain functions," right).

(B) Gain functions of 81 $_F$M and 148 $_F$S cones sorted along the x axis by "dark-light index," $DLi = (A_L-A_D)/(A_L+A_D)$.

(C) Average gain functions (shadings ±1 SEM).

(D) Enveloping histograms: *DLi* of cones (from B) with $_F$S cones plotted along an inverted y axis (violet). Darker bars: difference in distributions of $_F$M and $_F$S cones (positive: $_F$M dominance, negative: $_F$S dominance).

(E) Distribution of peak-to-peak amplitudes.

(F) Distribution of linear correlation coefficients between all pairs of individual gain functions within the populations of $_F$M and $_F$S cones.

See also Figure S4.

zero, indicating that $_F$S, but not $_F$M cones, preferentially encode dark over light contrasts (Figures 6B and 6D, $_F$S: −0.14 ± 0.37, $_F$M: 0.06 ± 0.29, $p < 0.001$, Wilcoxon rank-sum test). Therefore, owing to the asymmetric distribution of $_F$M and $_F$S cones along the retina's dorsoventral axis (Figure 4D), achromatic contrast coding in $_F$S and $_F$M cones is matched to the distribution of natural contrasts above and below the horizon (Figure 1C$_1$). DLi and SC weakly correlated across all recorded cones (rho = 0.22; $p < 0.05$), as was expected, simply because the DLi distributions for $_F$S and $_F$M cones differ (Figure 6D). However, within each of the two groups, we found no clear correlation ($rho_M = -0.06$; $p > 0.5$; $rho_S = 0.02$; $p > 0.5$), suggesting that the DLi is not directly related to SC. Also, neither DLi nor SC showed clear trends when plotted for each functional cone type as functions of cone position along the dorsoventral axis (data not shown). This is not too surprising, because the opsin transitional zone is rather narrow (see previous section).

Second, the average peak amplitudes of $_F$S responses were almost twice that of $_F$M responses (Figures 6C and 6E; $_F$S: 8.6 ± 6.1, $_F$M: 4.7 ± 2.8, $p < 0.001$ Wilcoxon rank-sum test), indicating that $_F$S cones exhibited a higher gain than $_F$M cones (Figures 6B and 6C). Notably, the higher gain of $_F$S cones may reflect an adjustment to the lower luminance of short-wavelength light in natural scenes.

Third, we quantified the heterogeneity of contrast encoding within each population by linear correlation of gain functions between all cone pairs. This revealed that $_F$S cones encoded contrast more heterogeneously than $_F$M cones, as indicated by lower correlation coefficients calculated between individual gain functions (Figure 6F).

## Optimal Sampling of Natural Contrasts

To what extent might the differential contrast sampling by the two functional cone types benefit contrast discrimination in corresponding regions of the visual field? In an information theoretical approach, Attneave (1954) and later Barlow (1961) suggested that sensory sampling should be directly linked to the distribution of input levels in the natural world. To allow a neuron to encode as much information as possible within its dynamic range, all response levels should be used equally often. Optimization is therefore achieved if a neuron's input-output

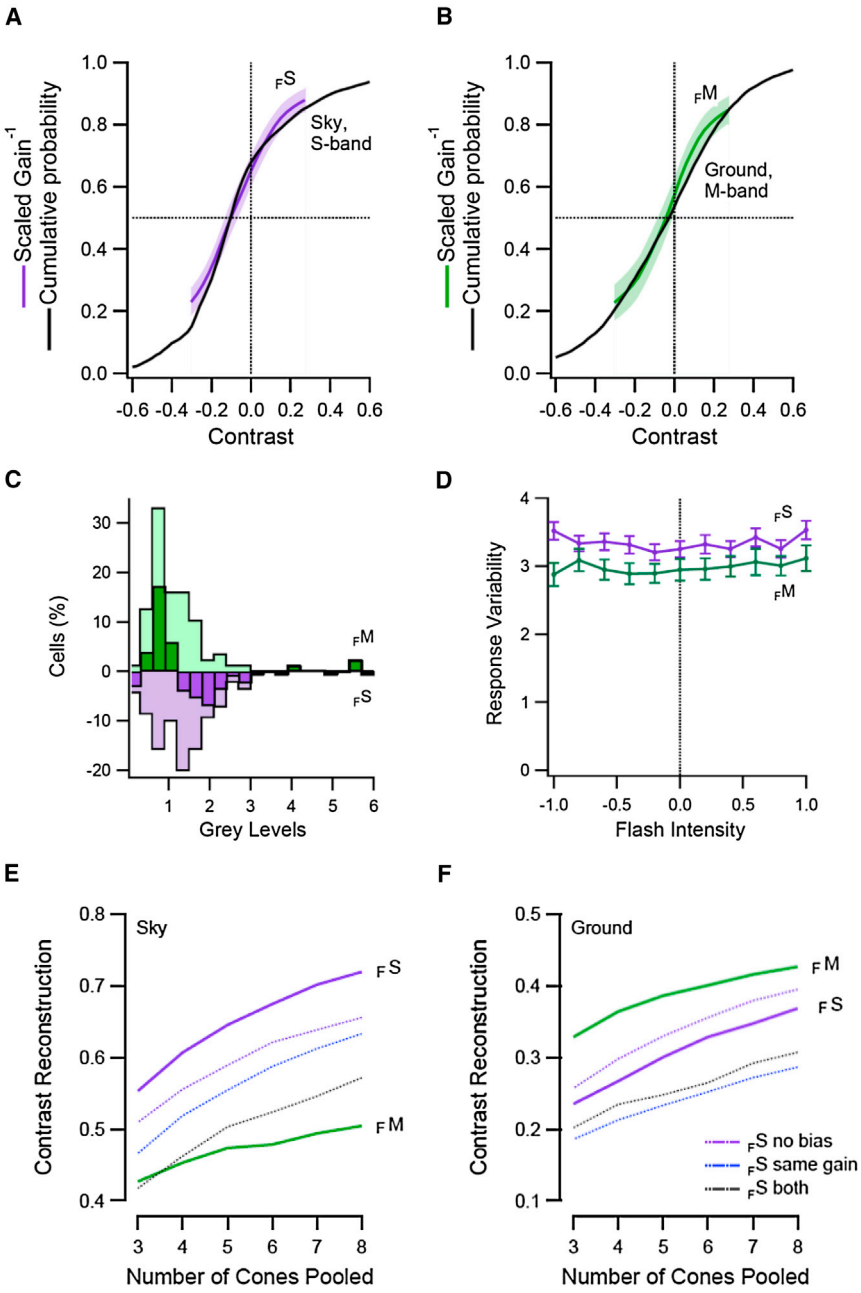


**Figure 7. Contrast Coding and Natural Statistics**

(A and B) Cumulative probability of natural contrasts (black) in the "S opsin band" sampled in the sky (A) and in the "M opsin band" on the ground (cf. Figure 1C$_1$). Superimposed are inverted average input-output functions of 148 $_F$S cones (A) and 81 $_F$M cones (B) (cf. Figure 6B). Shadings indicate 95% confidence limits.

(C) Distribution of gray levels encoded by $_F$M and $_F$S cones evaluated in Figures 6B and 6C.

(D) Response variability was independent of stimulus intensity ($p < 0.001$; errors in SEM).

(E and F) Solid lines: contrast reconstruction in sky and on ground by modeled second-order neurons (e.g., retinal bipolar cells) for different number of cones pooled. Dotted lines: $_F$S performance following additional manipulations of $_F$S cone gain functions: shifting of gain functions to yield DLi = 0 (purple); assuming gain ($_F$S) = gain ($_F$M) (blue); or both (black).

See also Figure S5.

function is equal to the cumulative probability distribution of the input (Barlow, 1961; Laughlin, 1981). To explore this link for mouse cones sampling the luminance distribution in the sky and on the ground, individual cone gain functions (Figure 6B) were inverted and amplitude-normalized based on extrapolated saturation points (Figures S5A and S5B). "Flash intensities" were converted into Weber contrast:

$$C = \left(I_S - I_B - I'_{S\ half}\right) \Big/ \left(I_B + I'_{S\ half}\right)$$

with $I_B$ denoting any background stimulation due to laser-related opsin excitation in the tissue and minimum stimulator light, and $I_S$ and $I'_{S\ half}$ corresponding to the absolute flash intensity and the half-maximal intensity of the light stimulus, respectively, with the latter corrected for minimum stimulator light (see Experimental Procedures; Figure S3). The resultant average input-output functions of $_F$S and $_F$M cones closely matched the cumulative probability functions of natural S-band contrasts in the sky and M-band contrasts on the ground, respectively (Figures 7A and 7B). Therefore, contrast sampling by $_F$S and $_F$M cones in the mouse retina closely approaches optimal sampling of the distribution of natural contrasts above and below the horizon, respectively.

What functional consequences may this sampling optimization bear toward contrast encoding by downstream retinal neurons? Ideal observer analysis (Smith and Dhingra, 2009) (see Experimental Procedures) of light- and dark-flash responses of individual cones (Figure 6B) revealed that $_F$S cones encoded more gray levels than $_F$M cones ($_F$S: 1.52 ± 1.05; $_F$M: 1.19 ± 0.89; $p = 0.042$ Wilcoxon rank-sum test; Figure 7C), in agreement with the larger response amplitudes measured in $_F$S cones compared with $_F$M cones (Figures 6C and 6E). In addition, $_F$M and $_F$S cones exhibited large differences in the slope and DLi of gain functions (Figure 6B). To explore the consequences of these differences, we set up a simple numerical model predicting "contrast reconstruction" of natural scene images by postsynaptic neurons summing inputs from individual $_F$M or $_F$S cones (see Experimental Procedures). Depending on their type, individual mouse bipolar cells integrate direct inputs from three to eight cones (Wässle et al., 2009). When keeping cone S/N at

the measured 1.52 and 1.19 for $_F$S and $_F$M cones, respectively (Figures 7C and 7D), and varying the number of cones pooled, $_F$S-driven model bipolar cells outperformed $_F$M-driven ones when reconstructing contrasts in the sky (Figure 7E), but on the ground $_F$M-driven bipolar cells outperformed $_F$S-driven ones (Figure 7F). Importantly, the improved performance of the $_F$S system in the sky appears to mainly depend on two key factors: (1) the preference of $_F$S cones for dark contrasts and (2) their higher gain (cf. Figures 6B–6E). When gain functions of all $_F$S cones were shifted by a constant offset to yield a mean DLi of zero, $_F$S performance decreased in the sky but increased on the ground (Figures 7E and 7F dotted purple lines). Second, when assuming the same gain in $_F$S cones as measured in $_F$M cones, $_F$S performance in both the sky and on the ground decreased (dotted blue lines). Combining both manipulations yielded a performance of the $_F$S system in the sky similar to that of the $_F$M system (dotted black lines).

## DISCUSSION

Our results demonstrate that already at the first synapse of the visual system the different light response properties of $_F$S and $_F$M cones, in combination with their spatial distribution along the mouse retina's dorsoventral axis, provide for near optimal sampling of achromatic contrasts above and below the horizon. Notably, it is not the match in "color" that makes $_F$S cones the better sensors for the sky region, as has been previously suggested (Gouras and Ekesten, 2004; Szél et al., 1994, 2000). Instead, it is the spectral tuning-independent properties of the predominant $_F$S cones in the ventral retina, namely, their dark bias, that enable them to encode achromatic contrasts that are prevalent in the sky region. Therefore, the mouse opsin gradient may serve to improve encoding of achromatic contrasts in the animal's visual environment.

### Anatomical versus Functional Cone Types in Mouse Retina

It is important to keep in mind that from the "evolutionary" point of view, there are—as in most mammals—two types of cones in the mouse: "true" S cones (Haverkamp et al., 2005) and cones that are homologous to M cones in other species. The great majority of mouse cones (the "evolutionary" M cones) coexpresses both S and M opsin at different ratios (Applebury et al., 2000; Nikonov et al., 2006; Wang et al., 2011). Because "true" S cones in mice so far can only be reliably identified via their synaptic connections with S cone-selective (type 9) bipolar cells (Haverkamp et al., 2005), we did not consider them separately, in neither our anatomical nor functional cone-type classification. "True" S cones are presumably included in the $_A$S and the $_F$S cones, together with dominantly S opsin-coexpressing MS cones. Importantly, this suggests that the functional differences in contrast coding between dorsal M opsin-dominated and ventral S opsin-dominated cones described here reflect a functional divergence between two subpopulations of the same coexpressing (evolutionary) cone type. This notion is further supported by two lines of evidence. First, the few $_F$S cones we recorded in the dorsal retina (n = 20), and which are expected to consist largely of "true" S cones, resembled $_F$M cones and not $_F$S cones in terms of gain and DLi (data not shown). Second, our functional data did not support the presence of a distinct $_F$MS cone phenotype (equivalent to the $_A$MS cones that can be defined based on opsin immunostaining). One explanation for this may be that the coexpressed opsins do not linearly contribute to cone function but that S opsin dominates. It is clear, though, that immunolabeling does not provide for reliable estimation of opsin activity ratios.

### Functional Differences within a Single Cone Type

The finding of functional differences between $_F$S and $_F$M cones, the majority of which belong to the M/S opsin-coexpressing cone type, is surprising. For the following reasons, we think that these differences are not assay-related artifacts. First, the transgenic mouse line used expresses TN-XL in all cone types, without any evidence for type-specific differences (Wei et al., 2012). Therefore, clipping and other nonlinearities in the TN-XL signal (for discussion, see Wei et al., 2012) are expected to be the same for $_F$S and $_F$M cones. Second, the effect of modulating two-photon excitation laser power on $_F$S and $_F$M cones was very small and not significantly different between the two functional cone types (for details, see legend of Figure S3). Third, electrical single-cell recordings from mouse cones showed that S opsin-dominated cones display higher gains than M opsin-dominated cones (Nikonov et al., 2006), consistent with our findings and with electrophysiological data from salamander cones (Rieke and Baylor, 2000) and mouse bipolar cells (Breuninger et al., 2011), as well as predictions from ERG measurements (Calderone and Jacobs, 1995; Jacobs and Williams, 2007).

What cellular or molecular mechanisms may underlie the functional differences between $_F$M and $_F$S cones? One obvious possible explanation is an endogenous difference in baseline $Ca^{2+}$ levels—i.e., the higher the resting level, the larger the light-induced suppression in $Ca^{2+}$. However, three findings argue against this explanation: First, baseline fluorescence ratio, which serves as estimate of baseline $Ca^{2+}$ level, did not differ for $_F$S and $_F$M cones (Figure S4A). Second, baseline fluorescence ratios did not correlate with DLi in either population of cones (Figure S4B). Third, light-evoked response amplitudes in both functional populations of cones increased with baseline fluorescence ratio (Figure S4C). Alternatively, contrast coding differences between $_F$M and $_F$S cones may result from a combination of differences in (1) the feedback that cones receive from horizontal cells (Jackman et al., 2011; Kamermans et al., 2001)—such feedback appears to remain largely intact in our slice preparation (Robin Kemmler, personal communication), (2) lateral spread of activity due to electrical cone-cone coupling (DeVries et al., 2002), and/or (3) heterogeneity in transduction cascade components, such as $Ca^{2+}$ buffers or voltage-activated channels expressed (Baylor, 1987; Beaumont et al., 2005). It is conceivable that not only the S opsin gene but also other genes are upregulated in $_F$S cones. For instance, the finding that in CACNA1F$^{-/-}$ mutant mice, in which a subunit of the L-type voltage-gated $Ca^{2+}$ channel is missing, dorsal cones die earlier than ventral cones (Zabouri and Haverkamp, 2013) may point at differences in the $Ca^{2+}$ channel complement between dorsal and ventral (and therefore $_F$M and $_F$S) cones. It will be interesting to investigate these possibilities in future studies.

### Color Vision versus Achromatic Use of Cone Types in the Mouse Retina

Contrary to popular perception, mice are far from blind. They see in daylight and are able to perform complex visual tasks (for review, see Huberman and Niell, 2011). Their retinal organization exhibits key similarities with that of the peripheral primate retina and a substantial portion of the mouse cortex is dedicated to vision (see also Zhang et al., 2012). Moreover, mice are not strictly nocturnal: recent investigations into the "natural" behavior of mice suggest that they indeed display diurnal activity, e.g., when natural food resources are restricted due to seasonal changes in the environment (Hut et al., 2011). In fact, also other rodent species that from their behavior in captivity were considered strictly nocturnal can switch to a diurnal activity pattern (e.g., Hoogenboom et al., 1984). Taken together, mice feature a fully functional cone system, including color vision (see below), and it would be surprising if they would not use it for orientation in their natural environment.

With the majority of cones coexpressing M and S opsin, one may wonder how mice are able to perceive color at all. But mice can perform color-discrimination tasks (Jacobs et al., 2004); they even display trichromatic color vision after the introduction of a third opsin gene (Jacobs et al., 2007). It is conceivable that chromatic processing in mice is restricted to the dorsal retina and a horizontal stripe of central retina. In dorsal retina, type 9 bipolar cells, which selectively contact "true" S cones (Haverkamp et al., 2005), can provide signals that are chromatically different to those in cone-unselective (or M cone-selective) bipolar cells, which will thereby be M opsin input dominated (Breuninger et al., 2011). In addition, RGCs that are located near the opsin transitional zone and receive input from both the S- and the M-dominated retinal domains, display chromatically opponent responses (Chang et al., 2013). However, in ventral retina chromatic processing is expected to be more difficult: while a small fraction of functional M cones remain (due to low S opsin coexpression), it is unclear if postsynaptic circuits are able to selectively tap into such cones to provide for chromatic opponency. In guinea pigs, which possess a (shallower) dorsoventral opsin gradient, ventral RGCs display reduced chromatic opponency (Yin et al., 2009). However, given the much more pronounced opsin coexpression, the ventral mouse retina may effectively be color blind. In this view, the visual field of mice is divided into three distinct functional domains: dorsal "normal" color vision involving dedicated M versus S circuits (reviewed in Neitz and Neitz, 2011), central large-scale spatial processing-dependent chromatic opponency (Chang et al., 2013), and a ventral achromatic zone that may serve primarily specific contrast detection tasks (Yin et al., 2006). It will be important to directly test the ability of mice to discriminate colors and achromatic contrast in these different visual fields in future behavioral studies.

### A Divided Retina with Different Functional Domains?

A static division into functionally distinct dorsal and ventral domains requires stable projection of the visual horizon onto the retina's nasotemporal axis, in particular, when the animal moves its body, head, and/or eyes. Most available data suggest that with respect to their eye movement repertoire, mice are not much different from other "afoveate" mammals (reviewed in Stahl, 2008). Hence, it is conceivable that eye movements of mice are at least partially of compensatory nature and assure that sky and ground reliably fall onto the ventral and dorsal retina, respectively, when the animal moves its head and/or body. Nevertheless, to date there is little systematic data on eye movements in freely roaming mice. Recent work on freely moving rats indicated that their eyes can move on surprisingly complex trajectories (Wallace et al., 2013), a result that if confirmed for mice needs to be considered in the context of their functionally divided retina.

In contrast to what has been proposed earlier (Gouras and Ekesten, 2004; Jacobs, 1993; Szél et al., 1994, 2000), our study suggests that it is not the match in "color" that makes S opsin-dominated mouse cones the better sensors for the sky region. Instead, the spectral tuning-independent properties of the functional S cones, namely, their dark bias and higher gain, qualify them to encode achromatic contrasts that are prevalent in the sky. This is supported not only by our contrast reconstruction model (Figures 7E and 7F), but also by our analysis of the entropy in different regions of "mouse-view" images (Figures 1D–1F). Surprisingly, the latter results suggests that, other than for the sky, the match between opsin type and spectral light distribution does matter for the ground region: here, the M band shows a higher entropy than the S band, suggesting that it is advantageous to "use" M-dominated cones to view the ground. However, in the context of achromatic contrasts above the horizon, why mice, unlike primates, feature UV-shifted S cones remains an open question.

It is noteworthy that the most numerous type of mouse RGC (W3) preferentially responds to small, dark stimuli, such as a bird in the sky, and appears to predominately exist in the ventral retina (Zhang et al., 2012), in striking agreement with the preference for dark contrasts in ventral cones. This link is somewhat tentative, as it cannot be ruled out at this stage if the reported ventral dominance of this RGC type may be related to spatially inhomogeneous GFP expression in the transgenic mouse line used rather than retinal segregation. In addition, the chromatic preference of these RGCs is currently unknown. Nonetheless, in combination with our results it appears that the visual system of the mouse has exquisitely adjusted its retinal feature extracting circuits to acknowledge specific visual feature distribution in natural scenes of its ground dwelling, shrubbery-covered terrestrial habitat. Why such a functional retina division, if indeed representing an advantage for survival, is not more widespread in animals occupying seemingly the same visual habitat (for discussion, see Peichl, 2005; Szél et al., 1994; Yilmaz and Meister, 2013) remains a matter of lively debate.

## EXPERIMENTAL PROCEDURES

### Calculation of Natural Statistics in Visual Scenes

Cone "activation sequences" ($5 \times 10^5$ points) were generated by taking estimated M or S opsin activation values (Figure S1B) at random from the upper and lower thirds of each "mouse-view" image (Figure 1A) for sky and ground, respectively. This "random walk" strategy was chosen to mimic single cone activation during head and eye movements as the animal surveys its visual environment. For each point, Weber contrast was calculated as $C = (P - P')/P'$, where $P$ is the current activation value, and $P'$ is mean

activation of the entire sequence. Therefore, $P'$ relates to a cone's adaptational state. We also calculated P′ as the average of the previous n "fixations" and found that contrast estimation was largely independent of n for n > 5. To calculate image entropy as an estimate of information contained at different regions of the "mouse-view" images, we rescaled monochromatic images to 8 bit. For each pixel, we calculated the brightness distribution (normalized to area = 1) of neighboring pixels over a range of ten pixels in each direction (yielding 21 × 21 = 441 pixel samples) and calculated local entropy H(x) as:

$$H(x) = -\sum_{i=1}^{n} p(xi) \cdot \ln p(xi)$$

where p is the fraction (0–1) of pixels falling into each bin (0–255) (Shannon, 1948).

### Animals and Tissue Preparation

All procedures were performed in accordance with the law on animal protection issued by the German Federal Government (Tierschutzgesetz) and approved by the institutional animal welfare committee of the University of Tübingen. For all experiments, we used 4- to 8-week-old homozygous transgenic mice (HR2.1:TN-XL) (Wei et al., 2012) that express the TN-XL $Ca^{2+}$ biosensor (Mank et al., 2006) under the control of the human red opsin promoter *hr2.1* (Wang et al., 1992) exclusively in cone photoreceptors. In these animals, TN-XL is expressed indiscriminately in all cones (Wei et al., 2012). Furthermore, cone function is not detectably hampered by TN-XL expression, as ERGs of HR2.1:TN-XL mice and wild-type littermates were indistinguishable.

Animals were housed under a standard 12 hr day/night rhythm. For $Ca^{2+}$ imaging, animals were dark-adapted for ≥2 hr. The eyes were quickly enucleated and hemisected in carboxygenated (95% $O_2$, 5% $CO_2$) artificial cerebral spinal fluid (ACSF) solution containing (in mM) 125 NaCl, 2.5 KCl, 2 $CaCl_2$, 1 $MgCl_2$, 1.25 $NaH_2PO_4$, 26 $NaHCO_3$, and 20 glucose (pH 7.4). The retina was dissected from the eyecup, cut in half, flattened, and mounted onto filter paper (0.8 μm pore size, Millipore) with photoreceptors facing up. Acute vertical slices (200 μm) were cut with a custom-made slicer. Slices with filter paper attached were stabilized using vacuum grease on coverslips, which were then placed under the microscope, where they were constantly perfused with temperated (~36°C) carboxygenated ACSF. Slices were always cut along the retina's principal axes (dorsal-ventral or temporal-nasal), and individual cone position was determined using the optic disk as a common landmark (Figure 4C). All procedures were carried out under very dim red light. Because the light-emitting diode (LED) ($\lambda_{LED}$ > 650 nm) used for illumination during dissection is expected to excite mouse cone opsins rather inefficiently (~$10^4$ times less M opsin excitation than at $\lambda_{M,peak}$), and the slices were allowed to recover in the recording chamber in complete darkness for ~30 min, we consider it unlikely that two cone opsins were differentially bleached prior to the recordings.

### Immunohistochemistry

Retinas (n = 3) with the orientation marked by a small dorsal cut were mounted onto filter paper (0.8 μm pore size, Millipore) and fixed in 4% paraformaldehyde (in PBS) for 15 min at 4°C. Immunolabeling was performed using antibodies against S opsin (goat anti-S opsin, 1:500, Santa Cruz Biotechnology), M opsin (rabbit anti-M opsin, 1:100, Chemicon), and GFP (chicken anti-GFP, 1:100, Acris) for 4 days. Secondary antibodies were Alexa Fluor conjugates (1:1,000, 12 hr, Invitrogen). For each retina 30–60 image stacks were taken at different retinal locations on a Zeiss Apotome (Image.Zi1) equipped with a 63× oil objective (1.4 NA) (Figure S2A). The precise retinal position of each image stack relative to the optic disc was subsequently determined based on bleach-zones in mosaic images of the complete retina taken with a 20× air objective (0.8 NA) (Figure S2E).

### Semiautomated Analysis of Immunolabeled Cone Outer Segments

Average projections of the M and S opsin channels from image stacks (see Immunohistochemistry) were Gauss-filtered, equalized for brightness and signal-to-noise ratio (8:1), and summed to generate a grayscale image comprising both channels. A threshold was applied using a Laplace operator (Dorostkar et al., 2010), and detected regions smaller than 1 $\mu m^2$ were discarded. For each remaining region, the mean intensities in individual M and S opsin channels were used to calculate an "M-S index" $MSi = (M - S)/(M + S)$ (for details, see Figure S2).

### Two-Photon $Ca^{2+}$ Imaging and Light Stimulation

We used a MOM-type two-photon microscope (designed by W. Denk, MPImF, Heidelberg; purchased from Sutter Instruments). Both design and procedures were described earlier ("eyecup scope," Euler et al., 2009). In brief, the system was equipped with a mode-locked Ti/sapphire laser (MaiTai-HP DeepSee, Newport Spectra-Physics) tuned to ~860 nm, two detection channels for fluorescence imaging of enhanced cyan fluorescent protein (eCFP) (483 BP 32; AHF) and citrine (535 BP 50), and a 20× objective (XLUMPlanFL, 0.95 NA, Olympus). For image acquisition, we used custom-made software (CfNT, by M. Müller, MPImF), taking 128 × 16 pixel images (31.25 frames/s) restricted to the cone terminals in the outer plexiform layer (Figure 3A, bottom). The use of vertical retinal slices avoided scanning of light-sensitive cone outer segments by the excitation laser and, thus, largely prevented opsin bleaching (as discussed in Wei et al., 2012).

The custom-built substage light stimulator (Breuninger et al., 2011) consisted of two band-pass-filtered ("blue": 360 BP 12, "green": 578 BP 10; AHF) LEDs, driven by an open-source microprocessor board (http://arduino.cc), and synchronized with the microscope's scanner retrace (Wei et al., 2012). The light from the LEDs was combined by a beam-splitter (400 DCLP, AHF) and focused by a condenser lens (0.8 NA, H DIC, Zeiss) through the bottom of the recording chamber. The light intensity (as photoisomerization rate, $10^3$ × P*$s^{-1}$/cone) generated by each of the stimulating LEDs ranged from 2 ($I_{S\ min}$: maximally "dark") to 12 ($I_{S\ max}$: maximally bright) for respective opsin and was calibrated as described previously (Breuninger et al., 2011; Chang et al., 2013). Because $I_{S\ min} > 0$, we correct $I_{S\ half}' = I_{S\ half} - I_{S\ min}$ and $I_{S\ max}' = I_{S\ max} - I_{S\ min}$, such that $I_{S\ min}$ can be considered as part of the background illumination $I_B$ (see below). We kept the cones light-adapted to a comparably bright LED background ($I_{S\ half}$ = 7 × $10^3$ P*$s^{-1}$/cone) that was adjusted to elicit equal photoisomerization rates for S and M opsins. A background illumination component ($I_B$) was always present, even when the "darkest" flashes were presented; it consisted of the LED background ($I_{S\ min}$) and a component generated by the scanning 2P excitation laser due to scattered laser light and emission fluorescence of recorded cone terminals ($I_L$), such that $I_B = I_{S\ min} + I_L$ (Figure S3). The $I_B$-related cone excitation was roughly estimated as ~$10^4$ × P*$s^{-1}$/cone, based on the transient $Ca^{2+}$ response to laser and stimulator background at the beginning of a recording epoch (Wei et al., 2012). For all experiments, slices were kept at $I_{S\ half}' + I_B$ for at least 30 s after the laser scanning started before stimuli were presented. Stimuli always covered the entire retinal slice.

### Analysis of Light-Evoked $Ca^{2+}$ Imaging Data

Regions of interest (ROIs) of individual cone terminals were manually placed and extracted over time as ΔR/R, with ratio $R = F_A/F_D$ of FRET acceptor (citrine) and donor (eCFP) fluorescence. Approximately 90% of the imaged cones displayed light responses to either or both stimulus wavelengths; the remaining 10% unresponsive cones often possessed abnormally high resting $Ca^{2+}$ levels (data not shown), indicative of cell damage likely due to the slicing procedure. To determine response quality and chromatic preference, we recorded light responses to a sinusoidal stimulus (with independently modulated blue and green components, see Figure 4$A_1$) in n = 3,208 cones and discarded all responses with S/N ratio below 3, leaving n = 1,996 cones. The average response to the sinusoidal stimulus (n = 6 trials) was used to calculate "spectral contrast," $SC = (R_G - R_B)/(R_G + R_B)$, where $R_G$ and $R_B$ denote the integral of the response to green and blue light, respectively (Figure 4$A_1$). Separations between functional M and S cones (see also Results) were defined based on the minima of a sum-of-two Gaussian fit to the SC histogram from n = 1,996 cones analyzed in 128 slices taken from 33 retinas (Figure 4$A_2$; threshold: 0; see also Assessing Quality of Cone-Type Distribution Fits).

### Assessing Quality of Cone-Type Distribution Fits

To test if the MSi (Figure 2$A_2$) and SC (Figure 4$A_2$) distributions are better explained by the presence of two or three cone types, the following statistical test

was performed. Randomly chosen, 90% of the (MSi or SC) data were fitted with the sum of two or three Gaussians, and then fit quality was tested with the remaining 10% of the data, and the BIC (Bayesian information criterion; Schwarz, 1978) was calculated:

$$BIC = n\,ln(\sigma_e^2) + k\,ln(n)$$

with the number of data points (n = 100) and the number of free parameters ($k$ = 6 for a 2- and $k$ = 9 for a three Gaussian fit). The error variance is defined as:

$$\sigma_e^2 = 1/n \sum \left(x_i - \underline{x}_i\right)^2$$

with $x_i$ the real data and $\underline{x}_i$ the estimate from the fit. We then repeated this cross-validation n = 200 times and plotted the BIC distributions for two and three Gaussian fits (Figures 2B and 4B; black and red curve, respectively; lower BIC indicates better fit).

### Ideal Observer Analysis and Contrast Reconstruction Model

We employed ideal observer analysis (Smith and Dhingra, 2009) to quantify the signal quality of individual cones (Figure 7C). An "ideal filter" (*if*) was derived by averaging cone responses to luminance steps and scaled to unit-correlation with itself:

$$if = \bar{r} / \left( \sqrt{\int_0^{1s} \bar{r}(t)^2\, dt} \right),$$

with $\bar{r}$ the time-dependent average cone response to light steps. Individual cone responses $(r)$ were then correlated with the "ideal filter" to determine response amplitudes $(a)$ :

$$a = \int_0^{1s} r(t) \cdot if(t)\, dt.$$

Mean and SD of the amplitude distribution were obtained by repeating the stimulation and used as proxies for signal and noise of an individual cone response, respectively. As response variability and stimulus intensity were largely independent (Figure 7D), the number of distinguishable gray levels of an individual cone equals the ratio of overall signal range to noise.

To assess contrast reconstruction by downstream retinal neurons, we set up a simple numerical model. First, we generated random "absorption" sequences (5 × $10^5$ points) in the M- and S-band taken from sky and ground pixels in "mouse-view" natural images (Figures 1A, $1D_1$, and 1E). For each of these four sequences, we calculated a "contrast sequence" (see Calculation of Natural Statistics in Visual Scenes above) as well as noise-added "response sequences" for each cone's normalized gain function, using the mean absorption value in a sequence as background. Added noise was equal to $1.19^{-1}$ and $1.52^{-1}$ for $_F$M and $_F$S cones, respectively (Figure 7C). Responses for each of 100 postsynaptic model neurons were taken as summed responses from n cones sampled at random from the population of $_F$M or $_F$S cones. "Contrast reconstruction" was calculated as the linear correlation coefficient times 100 between a contrast-sequence and the response-sequence of each postsynaptic neuron (Figures 7E and 7F).

### Data Analysis

All data analysis was performed using Igor-Pro 6.21 (Wavemetrics), MATLAB 7 (MathWorks), Image J (NIH, http://rsbweb.nih.gov/ij), and Amira (Visage Imaging).

## SUPPLEMENTAL INFORMATION

Supplemental Information includes five figures and can be found with this article online at http://dx.doi.org/10.1016/j.neuron.2013.09.030.

## AUTHOR CONTRIBUTIONS

Experiments were designed by T.B., T.S., and T.E. and performed by T.B., T.S., and M.Z. Data analysis was performed by T.B., T.S., L.C., and T.E. The transgenic mouse line was generated by T.W. and B.W. The manuscript was written by T.B., T.S., and T.E.

## ACKNOWLEDGMENTS

We thank Gordon Eske for technical assistance, Wadood Haq for helping to build the hyperspectral scanner, and Peter Dedecker (Division of Molecular Imaging and Photonics, Department of Chemistry of K.U. Leuven, Belgium) for providing the spectrometer IgorPro XOP. We thank Simon Laughlin (Department of Zoology, Cambridge, UK), Leo Peichl (MPI for Brain Research, Frankfurt/M., Germany) and Tanja Grau for helpful feedback on the manuscript, and Frank Schaeffel for stimulating discussions. This work was supported by DFG (FOR 701; EXC 307; KFO 134), BMBF (Bernstein Centre for Computational Neuroscience, Tübingen, FKZ:01GQ1002), the *fortüne* program (2125-0-0, Tübingen, Germany), and the Tistou und Charlotte Kerstan Stiftung, Germany.

Accepted: September 3, 2013
Published: December 4, 2013

## REFERENCES

Applebury, M.L., Antoch, M.P., Baxter, L.C., Chun, L.L., Falk, J.D., Farhangfar, F., Kage, K., Krzystolik, M.G., Lyass, L.A., and Robbins, J.T. (2000). The murine cone photoreceptor: a single cone type expresses both S and M opsins with retinal spatial patterning. Neuron *27*, 513–523.

Attneave, F. (1954). Some informational aspects of visual perception. Psychol. Rev. *61*, 183–193.

Barlow, H.B. (1961). Possible principles underlying the transformation of sensory messages. In Sensory Communication, W.A. Rosenblith, ed. (Cambridge: MIT Press), pp. 217–234.

Baylor, D.A. (1987). Photoreceptor signals and vision. Proctor lecture. Invest. Ophthalmol. Vis. Sci. *28*, 34–49.

Beaumont, V., Llobet, A., and Lagnado, L. (2005). Expansion of calcium microdomains regulates fast exocytosis at a ribbon synapse. Proc. Natl. Acad. Sci. USA *102*, 10700–10705.

Breuninger, T., Puller, C., Haverkamp, S., and Euler, T. (2011). Chromatic bipolar cell pathways in the mouse retina. J. Neurosci. *31*, 6504–6517.

Calderone, J.B., and Jacobs, G.H. (1995). Regional variations in the relative sensitivity to UV light in the mouse retina. Vis. Neurosci. *12*, 463–468.

Chang, L., Breuninger, T., and Euler, T. (2013). Chromatic coding from cone-type unselective circuits in the mouse retina. Neuron *77*, 559–571.

Denk, W., and Detwiler, P.B. (1999). Optical recording of light-evoked calcium signals in the functionally intact retina. Proc. Natl. Acad. Sci. USA *96*, 7035–7040.

Denk, W., Strickler, J.H., and Webb, W.W. (1990). Two-photon laser scanning fluorescence microscopy. Science *248*, 73–76.

DeVries, S.H., Qi, X., Smith, R., Makous, W., and Sterling, P. (2002). Electrical coupling between mammalian cones. Curr. Biol. *12*, 1900–1907.

Dorostkar, M.M., Dreosti, E., Odermatt, B., and Lagnado, L. (2010). Computational processing of optical measurements of neuronal and synaptic activity in networks. J. Neurosci. Methods *188*, 141–150.

Ekesten, B., and Gouras, P. (2005). Cone and rod inputs to murine retinal ganglion cells: evidence of cone opsin specific channels. Vis. Neurosci. *22*, 893–903.

Euler, T., Hausselt, S.E., Margolis, D.J., Breuninger, T., Castell, X., Detwiler, P.B., and Denk, W. (2009). Eyecup scope—optical recordings of light stimulus-evoked fluorescence signals in the retina. Pflügers Arch. Eur. J. Phys. *457*, 1393–1414.

Gouras, P., and Ekesten, B. (2004). Why do mice have ultra-violet vision? Exp. Eye Res. *79*, 887–892.

Haverkamp, S., Wässle, H., Duebel, J., Kuner, T., Augustine, G.J., Feng, G., and Euler, T. (2005). The primordial, blue-cone color system of the mouse retina. J. Neurosci. *25*, 5438–5445.

Hoogenboom, I., Daan, S., Dallinga, J.H., and Schoenmakers, M. (1984). Seasonal change in the daily timing of behaviour of the common vole, Microtus arvalis. Oecologia *61*, 18–31.

Huberman, A.D., and Niell, C.M. (2011). What can mice tell us about how vision works? Trends Neurosci. *34*, 464–473.

Hut, R.A., Pilorz, V., Boerema, A.S., Strijkstra, A.M., and Daan, S. (2011). Working for food shifts nocturnal mouse activity into the day. PLoS ONE *6*, e17527.

Jackman, S.L., Babai, N., Chambers, J.J., Thoreson, W.B., and Kramer, R.H. (2011). A positive feedback synapse from retinal horizontal cells to cone photoreceptors. PLoS Biol. *9*, e1001057.

Jacobs, G.H. (1993). The distribution and nature of colour vision among the mammals. Biol. Rev. Camb. Philos. Soc. *68*, 413–471.

Jacobs, G.H., and Williams, G.A. (2007). Contributions of the mouse UV photopigment to the ERG and to vision. Doc. Ophthalmol. *115*, 137–144.

Jacobs, G.H., Neitz, J., and Deegan, J.F., 2nd. (1991). Retinal receptors in rodents maximally sensitive to ultraviolet light. Nature *353*, 655–656.

Jacobs, G.H., Williams, G.A., and Fenwick, J.A. (2004). Influence of cone pigment coexpression on spectral sensitivity and color vision in the mouse. Vision Res. *44*, 1615–1622.

Jacobs, G.H., Williams, G.A., Cahill, H., and Nathans, J. (2007). Emergence of novel color vision in mice engineered to express a human cone photopigment. Science *315*, 1723–1725.

Kamermans, M., Fahrenfort, I., Schultz, K., Janssen-Bienhold, U., Sjoerdsma, T., and Weiler, R. (2001). Hemichannel-mediated inhibition in the outer retina. Science *292*, 1178–1180.

Karklin, Y., and Lewicki, M.S. (2009). Emergence of complex cell properties by learning to generalize in natural scenes. Nature *457*, 83–86.

Laughlin, S. (1981). A simple coding procedure enhances a neuron's information capacity. Z. Naturforsch., C, Biosci. *36*, 910–912.

Laughlin, S., and McGinness, S. (1978). The structures of dorsal and ventral regions of a dragonfly retina. Cell Tissue Res. *188*, 427–447.

Lyubarsky, A.L., Falsini, B., Pennesi, M.E., Valentini, P., and Pugh, E.N., Jr. (1999). UV- and midwave-sensitive cone-driven retinal responses of the mouse: a possible phenotype for coexpression of cone photopigments. J. Neurosci. *19*, 442–455.

Mank, M., Reiff, D.F., Heim, N., Friedrich, M.W., Borst, A., and Griesbeck, O. (2006). A FRET-based calcium biosensor with fast signal kinetics and high fluorescence change. Biophys. J. *90*, 1790–1796.

Neitz, J., and Neitz, M. (2011). The genetics of normal and defective color vision. Vision Res. *51*, 633–651.

Nikonov, S.S., Kholodenko, R., Lem, J., and Pugh, E.N., Jr. (2006). Physiological features of the S- and M-cone photoreceptors of wild-type mice from single-cell recordings. J. Gen. Physiol. *127*, 359–374.

Peichl, L. (2005). Diversity of mammalian photoreceptor properties: adaptations to habitat and lifestyle? Anat. Rec. A Discov. Mol. Cell. Evol. Biol. *287*, 1001–1012.

Prusky, G.T., and Douglas, R.M. (2008). Measuring vision in the awake behaving mouse. In Eye, Retina and Visual System of the Mouse, L.M. Chalupa and R.W. Williams, eds. (Cambridge: MIT Press), pp. 107–118.

Ratliff, C.P., Borghuis, B.G., Kao, Y.H., Sterling, P., and Balasubramanian, V. (2010). Retina is structured to process an excess of darkness in natural scenes. Proc. Natl. Acad. Sci. USA *107*, 17368–17373.

Rieke, F., and Baylor, D.A. (2000). Origin and functional impact of dark noise in retinal cones. Neuron *26*, 181–186.

Röhlich, P., van Veen, T., and Szél, A. (1994). Two different visual pigments in one retinal cone cell. Neuron *13*, 1159–1166.

Schaeffel, F. (2008). The mouse as a model for myopia, and optics of its eye. In Eye, Retina and Visual System of the Mouse, L.M. Chalupa and R.W. Williams, eds. (Cambridge: MIT Press), pp. 73–86.

Schwarz, G. (1978). Estimating the dimension of a model. Ann. Stat. *6*, 461–464.

Shannon, C.E. (1948). A mathematical theory of communication. Bell Syst. Tech. J. *27*, 379–423, 623–656.

Smith, R.G., and Dhingra, N.K. (2009). Ideal observer analysis of signal quality in retinal circuits. Prog. Retin. Eye Res. *28*, 263–288.

Stahl, J.S. (2008). Characteristics and applications of mouse eye movements. In Eye, Retina, and Visual System of the Mouse, L.M. Chalupa and R.W. Williams, eds. (Cambridge: MIT Press), pp. 87–105.

Szél, A., Röhlich, P., Caffé, A.R., Juliusson, B., Aguirre, G., and Van Veen, T. (1992). Unique topographic separation of two spectral classes of cones in the mouse retina. J. Comp. Neurol. *325*, 327–342.

Szél, A., Csorba, G., Caffé, A.R., Szél, G., Röhlich, P., and van Veen, T. (1994). Different patterns of retinal cone topography in two genera of rodents, Mus and Apodemus. Cell Tissue Res. *276*, 143–150.

Szél, A., Lukáts, A., Fekete, T., Szepessy, Z., and Röhlich, P. (2000). Photoreceptor distribution in the retinas of subprimate mammals. J. Opt. Soc. Am. A Opt. Image Sci. Vis. *17*, 568–579.

Tkačik, G., Garrigan, P., Ratliff, C., Milčinski, G., Klein, J.M., Seyfarth, L.H., Sterling, P., Brainard, D.H., and Balasubramanian, V. (2011). Natural images from the birthplace of the human eye. PLoS ONE *6*, e20409.

Wallace, D.J., Greenberg, D.S., Sawinski, J., Rulla, S., Notaro, G., and Kerr, J.N. (2013). Rats maintain an overhead binocular field at the expense of constant fusion. Nature *498*, 65–69.

Wang, Y., Macke, J.P., Merbs, S.L., Zack, D.J., Klaunberg, B., Bennett, J., Gearhart, J., and Nathans, J. (1992). A locus control region adjacent to the human red and green visual pigment genes. Neuron *9*, 429–440.

Wang, Y.V., Weick, M., and Demb, J.B. (2011). Spectral and temporal sensitivity of cone-mediated responses in mouse retinal ganglion cells. J. Neurosci. *31*, 7670–7681.

Wässle, H., Puller, C., Müller, F., and Haverkamp, S. (2009). Cone contacts, mosaics, and territories of bipolar cells in the mouse retina. J. Neurosci. *29*, 106–117.

Weckström, M., and Laughlin, S.B. (1995). Visual ecology and voltage-gated ion channels in insect photoreceptors. Trends Neurosci. *18*, 17–21.

Wei, T., Schubert, T., Paquet-Durand, F., Tanimoto, N., Chang, L., Koeppen, K., Ott, T., Griesbeck, O., Seeliger, M.W., Euler, T., and Wissinger, B. (2012). Light-driven calcium signals in mouse cone photoreceptors. J. Neurosci. *32*, 6981–6994.

Wyszecki, G., and Stiles, W.S. (2000). Color Science: Concepts and Methods, Quantitative Data and Formulae. (Hoboken: Wiley).

Yilmaz, M., and Meister, M. (2013). Rapid Innate Defensive Responses of Mice to Looming Visual Stimuli. Curr. Biol. *23*, 2011–2015.

Yin, L., Smith, R.G., Sterling, P., and Brainard, D.H. (2006). Chromatic properties of horizontal and ganglion cell responses follow a dual gradient in cone opsin expression. J. Neurosci. *26*, 12351–12361.

Yin, L., Smith, R.G., Sterling, P., and Brainard, D.H. (2009). Physiology and morphology of color-opponent ganglion cells in a retina expressing a dual gradient of S and M opsins. J. Neurosci. *29*, 2706–2724.

Zabouri, N., and Haverkamp, S. (2013). Calcium channel-dependent molecular maturation of photoreceptor synapses. PLoS ONE *8*, e63853.

Zhang, Y., Kim, I.J., Sanes, J.R., and Meister, M. (2012). The most numerous ganglion cell type of the mouse retina is a selective feature detector. Proc. Natl. Acad. Sci. USA *109*, E2391–E2398.